EUROPEAN ORGANIZATION FOR NUCLEAR RESEARCH

CERN-EP/90-32

9 March 1990

A PRECISE MEASUREMENT OF THE Z RESONANCE PARAMETERS THROUGH ITS HADRONIC DECAYS

DELPHI Collaboration

Abstract

A measurement of the cross-section for e^+e^- →hadrons using 11000 hadronic decays of the Z boson at ten different center-of-mass energies is presented.

A three-parameter fit gives the following values for the Z mass M_z, the total width Γ_z, the product of the electronic and hadronic partial widths $\Gamma_e\Gamma_h$, and the unfolded pole cross-section σ_0:

$$M_z = 91.171 \pm 0.030(stat.) \pm 0.030(beam)GeV$$

$$\Gamma_z = 2.511 \pm 0.065GeV$$

$$\Gamma_e\Gamma_h = 0.148 \pm 0.006(stat.) \pm 0.004(syst.)GeV^2$$

$$\sigma_0 = 41.6 \pm 0.7(stat.) \pm 1.1(syst.)nb$$

Good agreement with the predictions of the Standard Model is observed. From a two-parameter fit the number of massless neutrino generations is found to be: $N_\nu = 2.97 \pm 0.26$.Thus the hypothesis of a fourth neutrino with mass less than 40 GeV is excluded with 95% confidence level.

Combining the cross-section measurements with the ratio Γ_l/Γ_h reported in another DELPHI paper [31], the hadronic, leptonic and invisible widths are found to be:

$\Gamma_h = 1741 \pm 61MeV, \Gamma_l = 85.1 \pm 2.9MeV, \Gamma_h/\Gamma_l = 20.45 \pm 0.98, \Gamma_{inv} = 515 \pm 54MeV,$

in good agreement with the Standard Model.

P.Abreu[16], W.Adam[37], F.Adami[28], T.Adye[27], G.D.Alekseev[12], J.V.Allaby[7], P.Allen[36], S.Almehed[19], F.Alted[36], S.J.Alvsvaag[4], U.Amaldi[7], E.Anassontzis[3], W.D.Apel[13], B.Asman[32], C.Astor Ferreres[30], J.E.Augustin[15], A.Augustinus[7], P.Baillon[7], P.Bambade[15], F.Barao[16], G.Barbiellini[34], D.Yu.Bardin[12], A.Baroncelli[29], O.Barring[19], W.Bartl[37], M.J.Bates[25], M.Baubillier[18], K.H.Becks[39], C.J.Beeston[25], P.Beilliere[6], I.Belokopytov[31], P.Beltran[9], D.Benedic[8], J.M.Benlloch[36], M.Berggren[32], D.Bertrand[2], S.Biagi[17], F.Bianchi[33], J.H.Bibby[25], M.S.Bilenky[12], P.Billoir[18], J.Bjarne[19], D.Bloch[8], P.N.Bogolubov[12], D.Bollini[5], T.Bolognese[28], M.Bonapart[22], P.S.L.Booth[17], M.Boratàv[18], P.Borgeaud[28], H.Borner[25], G.Borisov[31], C.Bosio[29], O.Botner[35], B.Bouquet[15], M.Bozzo[10], S.Braibant[7], P.Branchini[29], K.D.Brand[39], R.A.Brenner[11], C.Bricman[2], R.C.A.Brown[7], N.Brummer[22], J.M.Brunet[6], L.Bugge[24], T.Buran[24], H.Burmeister[7], C.M.Buttar[25], J.A.M.A.Buytaert[2], M.Caccia[20], M.Calvi[20], A.J.Camacho Rozas[30], J.E.Campagne[7], A.Campion[17], T.Camporesi[7], V.Canale[29], F.Cao[2], L.Carroll[17], C.Caso[10], E.Castelli[34], M.V.Castillo Gimenez[36], A.Cattai[7], F.R.Cavallo[5], L.Cerrito[29], P.Charpentier[7], P.Checchia[26], G.A.Chelkov[12], L.Chevalier[28], C.Chiccoli[5], P.V.Chliapnikov[31], V.Chorowicz[18], R.Cirio[33], M.P.Clara[33], J.L.Contreras[36], R.Contri[10], G.Cosme[15], F.Couchot[15], H.B.Crawley[1], D.Crennell[27], M.Cresti[26], G.Crosetti[10], N.Crosland[25], M.Crozon[6], J.Cuevas Maestro[30], S.Czellar[11], S.Dagoret[15], E.Dahl-Jensen[21], B.D'Almagne[15], M.Dam[7], G.Damgaard[21], G.Darbo[10], E.Daubie[2], M.Davenport[7], P.David[18], A.De Angelis[34], M.De Beer[28], H.De Boeck[2], W.De Boer[13], C.De Clercq[2], M.D.M.De Fez Laso[36], N.De Groot[22], B.De Lotto[34], C.De La Vaissiere[18], C.Defoix[6], D.Delikaris[7], P.Delpierre[6], N.Demaria[33], K.G.Denisenko[12], L.Di Ciaccio[29], A.N.Diddens[22], H.Dijkstra[7], F.Djama[8], J.Dolbeau[6], K.Doroba[38], M.Dracos[8], J.Drees[39], M.Dris[23], W.Dulinski[8], R.Dzhelyadin[31], D.N.Edwards[17], L.O.Eek[35], P.A.M.Eerola[11], T.Ekelof[35], G.Ekspong[32], J.P.Engel[8], V.Falaleev[31], A.Fenyuk[31], M.Fernandez Alonso[30], A.Ferrer[36], S.Ferroni[10], T.A.Filippas[23], A.Firestone[1], H.Foeth[7], E.Fokitis[23], F.Fontanelli[10], H.Forsbach[39], B.Franek[27], K.E.Fransson[35], P.Frenkiel[6], D.C.Fries[13], R.Fruhwirth[37], F.Fulda-Quenzer[15], H.Fuerstenau[13], J.Fuster[7], J.M.Gago[16], G.Galeazzi[26], D.Gamba[33], U.Gasparini[26], P.Gavillet[7], S.Gawne[17], E.N.Gazis[23], P.Giacomelli[5], K.W.Glitza[39], R.Gokieli[18], V.M.Golovatyuk[12], A.Goobar[32], G.Gopal[27], M.Gorski[38], V.Gracco[10], A.Grant[7], F.Grard[2], E.Graziani[29], M.H.Gros[15], G.Grosdidier[15], B.Grossetete[18], S.Gumenyuk[31], J.Guy[27], F.Hahn[39], M.Hahn[13], S.Haider[7], Z.Hajduk[14], A.Hakansson[19], A.Hallgren[35], K.Hamacher[39], G.Hamel De Monchenault[28], J.F.Harris[25], B.Heck[7], I.Herbst[39], J.J.Hernandez[36], P.Herquet[2], H.Herr[7], E.Higon[36], H.J.Hilke[7], T.Hofmokl[38], R.Holmes[1], S.O.Holmgren[32], J.E.Hooper[21], M.Houlden[17], J.Hrubec[37], P.O.Hulth[32], K.Hultqvist[32], D.Husson[8], B.D.Hyams[7], P.Ioannou[3], P.S.Iversen[4], J.N.Jackson[17], P.Jalocha[14], G.Jarlskog[19], P.Jarry[28], B.Jean-Marie[15], E.K.Johansson[32], M.Jonker[7], L.Jonsson[19], P.Juillot[8], R.B.Kadyrov[12], G.Kalkanis[3], G.Kalmus[27], G.Kantardjian[7], F.Kapusta[18], P.Kapusta[14], S.Katsanevas[3], E.C.Katsoufis[23], R.Keranen[11], J.Kesteman[2], B.A.Khomenko[12], B.King[17], H.Klein[7], W.Klempt[7], A.Klovning[4], P.Kluit[2], J.H.Koehne[13], B.Koene[22], P.Kokkinias[9], M.Kopf[13], M.Koratzinos[7], K.Korcyl[14], B.Korzen[7], C.Kourkoumelis[3], T.Kreuzberger[37], J.Krolikowski[38], U.Kruener-Marquis[39], W.Krupinski[14], W.Kucewicz[20], K.Kurvinen[11], M.I.Laakso[11], C.Lambropoulos[9], J.W.Lamsa[1], L.Lanceri[34], D.Langerveld[22], V.Lapin[31], J.P.Laugier[28], R.Lauhakangas[11], P.Laurikainen[11], G.Leder[37], F.Ledroit[6], J.Lemonne[2], G.Lenzen[39], V.Lepeltier[15], A.Letessier-Selvon[18], E.Lieb[39], E.Lillestol[7], E.Lillethun[4], J.Lindgren[11], I.Lippi[26], R.Llosa[36], B.Loerstad[19], M.Lokajicek[12], J.G.Loken[25], A.Lopez[15], M.A.Lopez Aguera[30], D.Loukas[9], J.J.Lozano[36], R.Lucock[27], B.Lund-Jensen[35], P.Lutz[6], L.Lyons[25], G.Maehlum[7], J.Maillard[6], A.Maltezos[9], S.Maltezos[23], F.Mandl[37], J.Marco[30], J.C.Marin[7], A.Markou[9], L.Mathis[6], C.Matteuzzi[20], G.Matthiae[29], M.Mazzucato[26], M.Mc Cubbin[17], R.Mc Kay[1], E.Menichetti[33], C.Meroni[20], W.T.Meyer[1], M.Michael[23], W.A.Mitaroff[37], G.V.Mitselmakher[12], U.Mjoernmark[19], T.Moa[32], R.Moeller[21], K.Moenig[39], M.R.Monge[10], P.Morettini[10], H.Mueller[13], H.Muller[7], G.Myatt[25], F.Naraghi[18], U.Nau-Korzen[39], F.L.Navarria[5], P.Negri[20], B.S.Nielsen[21], M.Nigro[26], V.Nikolaenko[31], V.Obraztsov[31], R.Orava[11], A.Ostankov[31], A.Ouraou[28], R.Pain[18], K.Pakonski[14], H.Palka[14], T.Papadopoulou[23], L.Pape[7], P.Pasini[5], A.Passeri[29], M.Pegoraro[26], V.Perevozchikov[31], M.Pernicka[37], M.Pimenta[16], O.Pingot[2], C.Pinori[26], A.Pinsent[25], M.E.Pol[16], G.Polok[14], P.Poropat[34], P.Privitera[5], A.Pullia[20], J.Pyyhtia[11], P.Queru[12], A.A.Rademakers[22], D.Radojicic[25], S.Ragazzi[20], W.H.Range[17], P.N.Ratoff[25], A.L.Read[24], N.G.Redaelli[20], M.Regler[37], D.Reid[17], P.B.Renton[25], L.K.Resvanis[3], F.Richard[15], J.Ridky[12], G.Rinaudo[33], A.Romero[33], P.Ronchese[26], E.Rosenberg[1], E.Rosso[7], P.Roudeau[15], T.Rovelli[5], V.Ruhlmann[28], A.Ruiz[30], H.Saarikko[11], D.Sacco[29], Y.Sacquin[28], A.B.Sadovsky[12], E.Sanchez[36], E.Sanchis[36], M.Sannino[10], A.A.Sazonov[12], M.Schaeffer[8], H.Schneider[13], F.Scuri[34], A.Sebastia[36], A.M.Segar[25], R.Sekulin[27], M.Sessa[34], G.Sette[10], R.Seufert[13], R.C.Shellard[7],

P.Siegrist[28], P.Simone[33], S.Simonetti[10], F.Simonetto[26], T.B.Skaali[24], J.Skeens[1], G.Skjevling[24], G.Smadja[28], G.R.Smith[27], R.Sosnowski[38], K.Spang[21], T.Spassoff[12], E.Spiriti[29], S.Squarcia[10], H.Staeck[39], C.Stanescu[29], G.Stavropoulos[9], F.Stichelbaut[2], A.Stocchi[20], J.Strauss[37], R.Strub[8], C.Stubenrauch[7], M.Szczekowski[38], M.Szeptycka[38], P.Szymanski[38], S.Tavernier[2], E.Tchernyaev[31], G.Theodosiou[9], A.Tilquin[6], J.Timmermans[22], L.G.Tkatchev[12], T.Todorov[12], D.Z.Toet[22], L.Tortora[29], D.Treille[7], U.Trevisan[10], G.Tristram[6], C.Troncon[20], E.N.Tsyganov[12], M.Turala[14], R.Turchetta[8], M.L.Turluer[28], T.Tuuva[11], I.A.Tyapkin[12], M.Tyndel[27], S.Tzamarias[7], F.Udo[22], S.Ueberschaer[39], V.A.Uvarov[31], G.Valenti[5], E.Vallazza[33], J.A.Valls[36], G.W.Van Apeldoorn[22], P.Van Dam[22], W.K.Van Doninck[2], N.Van Eijndhoven[7], C.Vander Velde[2], J.Varela[16], P.Vaz[16], G.Vegni[20], M.E.Veitch[25], E.Vela[36], J.Velasco[36], L.Ventura[26], W.Venus[27], F.Verbeure[2], L.S.Vertogradov[12], L.Vibert[18], D.Vilanova[28], L.Viseu Melo[16], E.V.Vlasov[31], A.S.Vodopianov[12], M.Vollmer[39], G.Voulgaris[3], M.Voutilainen[11], V.Vrba[12], H.Wahlen[39], C.Walck[32], F.Waldner[34], M.Wayne[1], P.Weilhammer[7], J.Werner[39], A.M.Wetherell[7], J.H.Wickens[2], J.Wikne[24], W.S.C.Williams[25], M.Winter[8], G.Wormser[15], K.Woschnagg[35], N.Yamdagni[32], A.Zaitsev[31], A.Zalewska[14], P.Zalewski[38], E.Zevgolatakos[9], G.Zhang[39], N.I.Zimin[12], R.Zitoun[18], R.Zukanovich Funchal[6], G.Zumerle[26], J.Zuniga[36]

(Submitted to Physics Letters B)

[1]Ames Laboratory and Department of Physics, Iowa State University, AMES IA 50011, U. S. A.
[2]Physics Department, Univ. Instelling Antwerpen, Universiteitsplein 1, B-2610 WILRIJK.
IIHE, ULB-VUB, Pleinlaan 2, B-1050 BRUXELLES.
Service de Phys. des Part. Elém., Faculté des Sciences, Université de l'Etat Mons, Av. Maistriau 19, B-7000 MONS.
[3]Physics Laboratory, University of Athens, Solonos Str. 104, GR-10680 ATHENS.
[4]Department of Physics, University of Bergen, Allégaten 55, N-5007 BERGEN.
[5]Dipartimento di Fisica, Università di Bologna and INFN, Via Irnerio 46, I-40126 BOLOGNA.
[6]Collège de France, Lab. de Physique Corpusculaire, 11 pl. M. Berthelot, F-75231 PARIS CEDEX 5.
[7]CERN, CH-1211 GENEVA 23.
[8]Division des Hautes Energies, CRN - Groupe DELPHI, B.P. 20 CRO, F-67037 STRASBOURG CEDEX.
[9]Greek Atomic Energy Commission, Nucl. Research Centre Demokritos, P.O. Box 60228, GR-15310 AGHIA PARASKEVI.
[10]Dipartimento di Fisica, Università di Genova and INFN, Via Dodecaneso 33, I-16146 GENOVA.
[11]Dept. of High Energy Physics, University of Helsinki, Siltavuorenpenger 20 C, SF-00170 HELSINKI 17.
[12]Joint Institute for Nuclear Research, Dubna, Head Post Office, P.O. Box 79, 101 000 MOSCOW, U.R.S.S.
[13]Institut für Experimentelle Kernphysik, Universität Karlsruhe, Postfach 6980, D-7500 KARLSRUHE 1.
[14]High Energy Physics Laboratory, Institute of Nuclear Physics, Ul. Kawiory 26 a, PL-30055 KRAKOW 30.
[15]Université de Paris-Sud, Lab. de l'Accélérateur Linéaire, Bat 200, F-91405 ORSAY.
[16]LIP, Av. Elias Garcia 14 - 1e, P-1000 LISBOA CODEX.
[17]Department of Physics, University of Liverpool, P.O. Box 147, GB - LIVERPOOL L69 3BX.
[18]LPNHE, Universités Paris VI et VII, Tour 33 (RdC), 4 place Jussieu, F-75230 PARIS CEDEX 05.
[19]Department of Physics, University of Lund, Sölvegatan 14, S-22363 LUND.
[20]Dipartimento di Fisica, Università di Milano and INFN, Via Celoria 16, I-20133 MILANO.
[21]Niels Bohr Institute, Blegdamsvej 17, DK-2100 COPENHAGUE 0.
[22]NIKHEF-H, Postbus 41882, NL-1009 DB AMSTERDAM.
[23]National Technical University, Physics Department, Zografou Campus, GR-15773 ATHENS.
[24]Physics Department, University of Oslo, Blindern, N-1000 OSLO 3.
[25]Nuclear Physics Laboratory, University of Oxford, Keble Road, GB - OXFORD OX1 3RH.
[26]Dipartimento di Fisica, Università di Padova and INFN, Via Marzolo 8, I-35131 PADOVA.
[27]Rutherford Appleton Laboratory, Chilton, GB - DIDCOT OX11 OQX.
[28]CEN-Saclay, DPhPE, F-91191 GIF-SUR-YVETTE CEDEX.
[29]Istituto Superiore di Sanità, Ist. Naz. di Fisica Nucl. (INFN), Viale Regina Elena 299, I-00161 ROMA.
Dipartimento di Fisica, Università di Roma II and INFN, Tor Vergata, I-00173 ROMA.
[30]Facultad de Ciencias, Universidad de Santander, av. de los Castros, E - 39005 SANTANDER.
[31]Inst. for High Energy Physics, P.O. Box 35, Protvino, SERPUKHOV (Moscow Region), U.R.S.S.
[32]Institute of Physics, University of Stockholm, Vanadisvägen 9, S-113 46 STOCKHOLM.
[33]Dipartimento di Fisica Sperimentale, Università di Torino and INFN, Via P. Giuria 1, I-10125 TORINO.
[34]Dipartimento di Fisica, Università di Trieste and INFN, Via A. Valerio 2, I-34127 TRIESTE.
Istituto di Fisica, Università di Udine, I-33100 UDINE.
[35]Department of Radiation Sciences, University of Uppsala, P.O. Box 535, S-751 21 UPPSALA.
[36]Inst. de Fisica Corpuscular IFIC, Centro Mixto Univ. de Valencia-CSIC, Avda. Dr. Moliner 50, E-46100 BURJASSOT (Valencia).
[37]Institut für Hochenergiephysik, Öesterreich Akad. d. Wissensch., Nikolsdorfergasse 18, A-1050 VIENNE.
[38]Inst. Nuclear Studies and, University of Warsaw, Ul. Hoza 69, PL-00681 WARSZAWA.
[39]Fachbereich Physik, University of Wuppertal, Postfach 100 127, D-5600 WUPPERTAL 1.

1. INTRODUCTION

The first 'fine' scan of the Z–resonance at the CERN Large Electron Positron Collider (LEP) has been completed. The measurement of the Z production cross section performed by the DELPHI Collaboration at ten different collision energies is presented here. The measured line–shape is interpreted in the context of the Standard Model. The data correspond to an integrated luminosity of 573 nb^{-1}, about 10 times more than the integrated luminosity for which results were reported in our previous publication [1]. Other measurements of the Z properties obtained in e^+e^- collisions may be found in ref. [2].

The selection criteria for both multihadronic and small angle Bhabha events are similar to those used in ref. [1]. However, for the selection of multihadronic events an alternative set of cuts was added in order to reduce the systematic uncertainties (sect. 5). The uncertainties of the luminosity measurement were reduced by a modification of the detector as well as by a more elaborate analysis (sect. 3).

2. APPARATUS

The features of the DELPHI apparatus which were relevant for the present analysis are listed in ref. [1]. For completeness they are recalled here, with the modifications necessary to cover the longer running period. Many different subdetectors are involved in this measurement.

- The **Inner Detector** is a cylindrical drift chamber (inner radius = 12 cm, outer radius = 28 cm) covering polar angles between 29° and 151°. A jet–chamber section providing 24 rϕ coordinates is surrounded by 5 layers of proportional chambers providing rϕ and longitudinal coordinates. These five layers were used in the trigger.

- The **Time Projection Chamber** (TPC) is a cylinder with 30 cm inner and 122 cm outer radius and a length of 2.7 m. For polar angles between 21° and 159° at least 4 space points are available for track reconstruction, while for angles between 39° and 141° up to 16 space points can be used.

- The **Outer Detector** has five layers of drift cells at a radius between 198 and 206 cm and covers polar angles from 42° to 138°. All layers provide precise rϕ coordinates and were used in the trigger.

- The **High Density Projection Chamber** (HPC) measures electromagnetic energy with high granularity over polar angles from 40° to 140°. It has a segmentation in depth of nine layers. For fast triggering, a scintillator layer is located behind the first five radiation lengths.

- About one third of the data were taken with the **Superconducting Solenoid** operating at a reduced field of 0.7 T. The rest of the data were taken at the design value of 1.2 T.

- The **Time Of Flight** (TOF) system is composed of a single layer of 172 counters surrounding the solenoid, and covering 41° to 139° in polar angle. It was used in the fast triggering.

- The **Electromagnetic Calorimeter** in the endcaps (FEMC) consists of 2 x 4500 lead glass blocks (granularity = 1° x 1°) with phototriode read out, covering polar angles from 10° to 35.5° and from 144.5° to 170°.

- The **Small Angle Tagger** calorimeters (SAT) cover polar angles from 43 to 135 mrad in both endcaps. They are composed of alternating layers of lead sheets – concentric with the beam axis – and scintillating fibres running parallel to the beam. Behind each calorimeter the fibers are collected into 288 bundles, each read out by a photodiode. The resulting segmentation is shown in Fig. 1. The calorimeters have inner and outer radii of 10 and 34.5 cm. The inner six rings of readout elements have radial extensions of 3 cm, the outer two 3.25 cm. The azimuthal coverage is 2π except for a small dead region, 2 cm wide, which appears at the vertical junction of the two half–cylinders. The inner four rings have an azimuthal segmentation of 15°, the outer four rings of 7.5 °. In order to define the inner radius of the acceptance region with high precision, one of the calorimeters was masked off by a 10 radiation length thick lead ring. The first third of the data were taken with a mask of maximum outer radius of 12 cm, whereas the remaining two thirds were taken with a 13 cm mask. The data taken with the 12 and 13 cm masks will be referred as samples A and B, respectively.

The masks had conical outer surfaces pointing back to the nominal interaction point. The diameters of the masks are known with a precision of better than 100 microns.

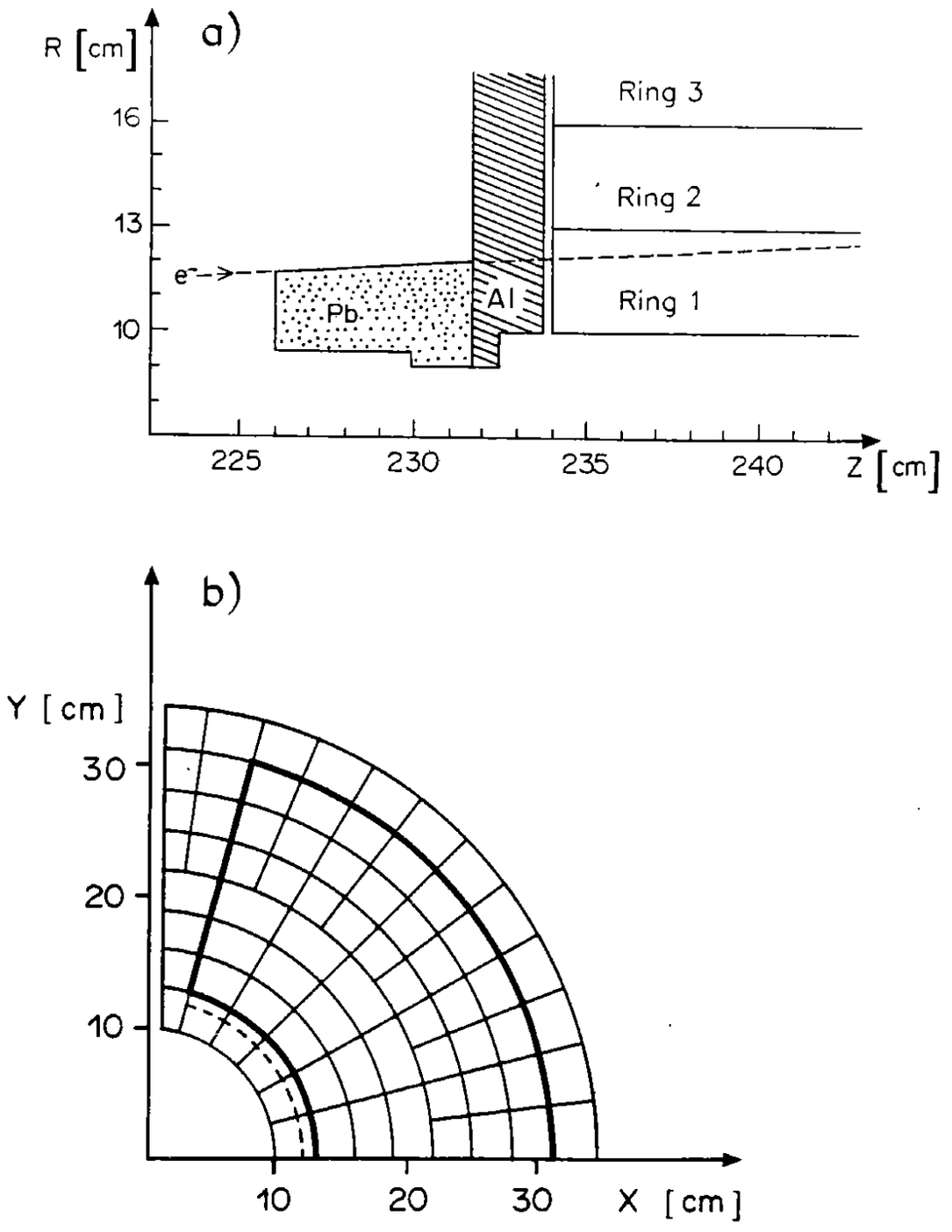

Fig. 1 – The Small Angle Tagger calorimeter. (a) Side view showing the 12 cm lead mask in front of calorimeter 2. (b) Segmentation of calorimeter in one quadrant. The border of the acceptance in calorimeter 2 is indicated by a thick line (dashed line for 12 cm mask).

3. LUMINOSITY MEASUREMENT

The luminosity measurement relied on the detection of small angle Bhabha events in the SAT. The triggers were based on analog sums of 24 channels arranged in 24 overlapping sectors of 30° per endcap (Fig. 1). The primary trigger required coplanar coincidence of energy depositions larger than about 15 GeV. A second trigger, based on an alternative set of discriminators, was operated at a threshold of about 35 GeV and did not include the coplanarity requirement. Two data taking periods were dedicated to the study of the luminosity trigger efficiency, with a single arm trigger (requiring only energy deposition in one calorimeter) added to the normal triggers.

Comparison of the performance of the first two triggers showed that the electronics and logic of the primary trigger were more than 99.9% effective. All 422 Bhabha events observed during the single arm runs satisfied the primary trigger condition. It follows that the trigger efficiency was greater than 99.4% at the 90% confidence level. A conservative value of 0.6% was taken as systematic uncertainty on the 100% trigger efficiency, since it was not measured directly during normal data taking.

The first step of the event selection was the formation of energy clusters in the calorimeters. Clusters were composed of at least three neighbouring readout elements, each with an energy response more than three standard deviations above the pedestal (typically 0.5 GeV). In case several clusters were found in one calorimeter, the cluster with the maximum number of elements (referred to later as the *primary cluster*) was used in the subsequent event selection. The energy barycentre was used to define the radial (r) and azimuthal (ϕ) coordinates of the shower. An acoplanarity cut of 20° was applied by using the azimuthal coordinates of the primary clusters detected in the two calorimeters.

Due to the steep angular dependence of the Bhabha cross section, a precise determination of the minimum scattering angle is crucial. In this experiment this was defined by the outer radius of the mask described in sect. 2. The other borders of the acceptance (Fig. 1) were defined by the requirement for the primary energy cluster in the masked calorimeter to be more than one 15° sector away from the vertical dead region and within the first 7 rings of the calorimeter. It has been estimated that the uncertainties in the knowledge of the internal geometry of the calorimeter introduce a 1% systematic uncertainty associated with these last two cuts. The ϕ–cut is by far the most important one. The systematic error of 1% would correspond to a shift of about 2.5 mm on the azimuthal position of the border between cells.

The purpose of the mask is to prevent electrons below a precisely defined scattering angle from depositing their full energy in the calorimeter. Monte Carlo studies show that already 300 microns inside the outer edge of the mask, it absorbs more than 60% of the energy of 45 GeV electrons. In order to reject electrons which hit the inner surface of the calorimeter after passing through the central hole of the mask, the quantity R was introduced. It is defined as the ratio between the energy deposited in the first ring of the masked calorimeter (calorimeter 2) to the total energy E_2 of the corresponding shower.

The distributions of the fractional energy E_2/E_{beam} versus R are shown in Figs 2(a) and (c), for samples A and B, respectively. They were made after an energy cut in calorimeter 1 of

$0.75 \leq E_1/E_{beam} \leq 1.5$. The Monte Carlo prediction for the conditions of sample A (12 cm mask) is plotted in Fig. 2(b). The cluster of events at $R \approx 0.9$ and $E_2/E_{beam} \approx 0.4$ is due to electrons which hit the mask. The band of events at $R \approx 1$ which extends to large energies is due to electrons which passed through the hole of the mask. The combined cut in R and E_2/E_{beam} indicated by the dashed line rejects both types of events. The separation between the signal and the background is better for sample B, shown in Fig. 2(c), since the 13 cm mask completely covers ring 1 of the calorimeter.

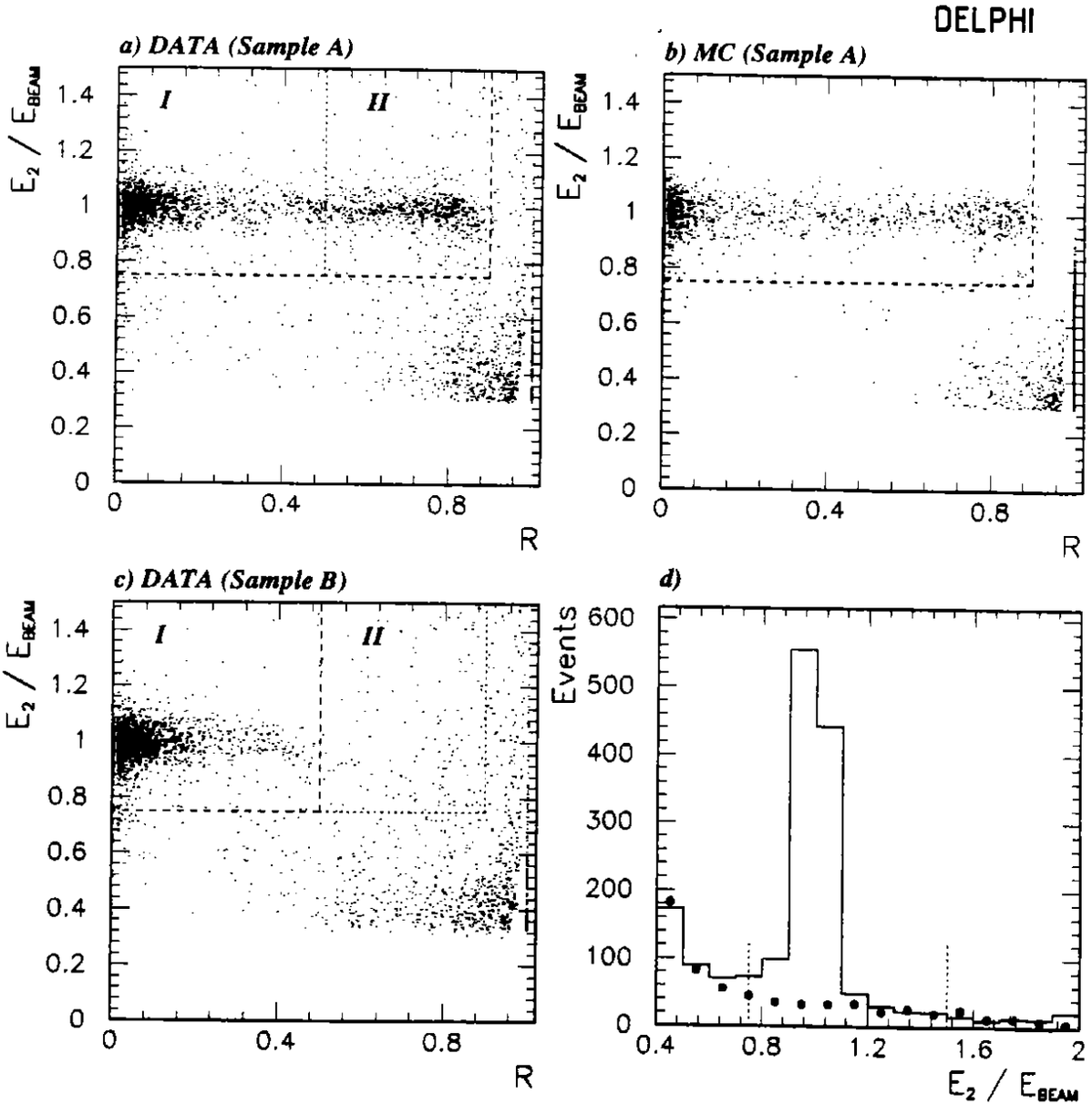

Fig. 2 – (a)–(c) Distribution of the energy ratio E_2/E_{beam} versus the energy fraction R (see text for the definition of R). (d) shows E_2/E_{beam} of sample A (continuous line) and B (dots) for $0.5 < R < 0.9$ normalized to the same luminosity.

For both samples a distributed background of events is observed. This is understood as being caused by showers which leaked through the back corner of the calorimeter into the photodiodes, simulating high energy depositions. In region I, this was estimated to be $(0.5 \pm 0.5)\%$ of the total number of Bhabha events (the same in both samples). However, in sample A the signal extends up to $R \approx 0.9$, as predicted by the Monte Carlo. The background in region II is larger and was subtracted using the signal–free data of sample B in region II. Fig. 2(d) shows the energy distributions of the events of sample A (continuous line) and B (dots) for $0.50 \leq R \leq 0.90$ normalized to the same luminosity. The background of sample A is well reproduced by the data of sample B. This procedure leads to a statistical background subtraction of 2.5% in the region II for sample A. A conservative systematic uncertainty of 1.3% was assigned to this subtraction. In summary, the background subtraction for sample A amounts to $(3.0 \pm 1.5)\%$ and for sample B to $(0.5 \pm 0.5)\%$, when selecting the events within the limits $0.75 \leq (E_1/E_{beam}, E_2/E_{beam}) \leq 1.5$.

A 1% total uncertainty on the integrated luminosity was estimated to originate from the above energy cuts by considering the following:

- The overall and cell to cell calibrations of the calorimeters were performed with a sample of Bhabha events. Applying different algorithms resulted in 0.3% variations in the integrated luminosity.
- Variation of the minimum energy cut (viz. 75% of the beam energy) by ± 5% changed the integrated luminosity by 0.5%.
- Based on an analysis of the single arm trigger data and the acoplanarity distribution of the full data sample, the background of off–momentum electrons was estimated to be less than 0.2%.

Due to the asymmetric geometric acceptance criteria and the azimuthal symmetry of the acceptance region, the sensitivity of the visible cross section to possible variations of the position of the interaction point in the transverse plane is negligible. However, the visible cross section is linearly sensitive to longitudinal displacements along the beam axis (i.e. z axis). The average z–position of the interaction region was measured with tracks from the hadronic Z–decay sample and was used to correct the data for each LEP machine fill. The corrections were typically 0.5% or less. A remaining 5 mm uncertainty on the absolute position of the mask relative to the interaction region would result in a 0.5% uncertainty on the visible cross section.

The visible cross section for the luminosity events was evaluated by a detector simulation [3] of Bhabha scattering events. An event generator that includes electroweak and radiative corrections to first order in α was used [4]. The hadronic vacuum polarization was updated according to ref. [5]. The lack of higher order corrections in the generator is assumed to give a 1% uncertainty on the theoretical cross section. The energy dependence of the cross section was evaluated by generating events at the 10 energy points of the scan with an approximate simulation of the event selection. These cross–sections were renormalized to the value obtained at $\sqrt{s} = 91.1$ GeV, the center–of–mass energy at which the full detector simulation was performed. The visible cross–sections at this energy were found to be 32.5 nb for sample A and 26.6 nb for sample B.

An uncertainty of 1% was estimated due to imperfections of the Monte Carlo modeling. The luminosity was computed assuming a Z mass (which enters the γZ interference term) of 91.1 GeV. The uncertainty on M_Z has a negligible effect on the luminosity calculation.

A summary of the systematic uncertainties on the luminosity measurement is given in Table 1. The overall uncertainty is 2.7% for sample A (6964 selected events), and 2.3% for sample B (9749 selected events), which results in a 2.4% uncertainty on the total sample. This is less than the 5% uncertainty reported in ref. [1] mainly because of the new measurement of the trigger efficiency, the improvement in the data quality resulting from the increase of the mask radius from 12 to 13 cm, and the correction for the vertex position.

TABLE 1 – Contributions to the uncertainty of the luminosity measurement

Contribution	%
Trigger efficiency	0.6
ϕ–cut	1.0
Energy cut	1.0
Interaction point position	0.5
Background subtraction B (A)	0.5 (1.5)
MC modeling	1.0
MC statistics	0.6
Theory	1.0
Total, sample B (A)	2.3 (2.7)

4. HADRONIC EVENT TRIGGER

In the barrel region, the trigger for hadronic events was based on two independent components:

(a) A 'track trigger' was made by coincidences of the ID and OD chambers. Each detector provided signals for charged particles with hits in 3 out of 5 layers. A back to back coincidence of OD quadrants together with any signal from the ID formed a trigger.

(b) A 'scintillator trigger' was made by coincidences of the HPC and TOF scintillation counters. Individual counters of both detectors were arranged in two groups of four quadrants placed symmetrically upstream and downstream of the crossing point. The HPC counters were sensitive to electromagnetic showers with an energy larger than 2 GeV while the TOF counters were sensitive to minimum ionizing particles penetrating the electromagnetic calorimeter and the coil.

The 'scintillator trigger' was the OR of the following subtriggers:

- coincidences of back to back TOF quadrants
- at least 3 TOF quadrants
- at least 2 HPC quadrants
- coincidence of any TOF with any HPC quadrant.

The exact knowledge of the trigger efficiency for events with a sphericity axis between 50° and 130° is crucial for the determination of the overall acceptance (sect. 5). Having recorded the trigger pattern event by event, we determined the efficiency of each subtrigger in the barrel region for hadronic events by using its redundancy with other subtriggers. From this measurement the following efficiencies for hadronic events with a sphericity axis between 50° and 130° were obtained:

- 'track trigger': $99.1 \pm 0.1\%$,
- 'scintillator trigger': $99.6 \pm 0.1\%$.

The inefficiency of the overall trigger in the barrel region was therefore less than 0.1 %.

To enhance the number of Z events with a sphericity axis pointing to the endcaps a calorimeter trigger based on the FEMC was added. It required a minimum energy deposition of 3 GeV in each endcap. Its contribution was included in the calculation of the global detection efficiency as described in sect. 5.

Approximately 9% of the data were recorded with one of the trigger components missing. The corresponding correction applied to the overall acceptance was $2.0 \pm 0.2\%$ in events taken with a missing ID, OD or TOF trigger and $1.0 \pm 0.1\%$ when the HPC or the FEMC triggers were absent. The resulting losses in trigger efficiency are larger for events with a sphericity axis outside the range from 50° to 130°.

Hadronic and Bhabha events were recorded with the same trigger- and data acquisition system in order to ensure equal live times.

5. HADRONIC EVENT SELECTION

Two different analyses have been performed:

The first analysis (A) relied only on charged particle tracks, whereas the second (B) used the energy deposition in the barrel electromagnetic calorimeter (HPC) in addition.

Both methods used the following selection criteria for charged particles:

- polar angle θ between 20° and 160°,
- momentum p between 0.1 GeV/c and 50 GeV/c,
- track length above 30 cm,
- relative error on momentum measurement below 100%,
- projection of impact parameter in the xy plane below 4 cm,
- z coordinate at the origin below 10 cm.

Analysis A:

Hadronic events were selected by requiring at least 3 tracks in one hemisphere (viz. $\theta < 90°$ or $\theta > 90°$) and a sum of the p_T^2 of all tracks relative to the beam axis greater than 9 GeV^2.

The multiplicity cut removed cosmic events and leptonic decays with the exception of a small fraction of $\tau^+\tau^-$ events. The p_T^2 cut rejected the contamination by beam gas and two photon interactions. Its value was chosen in order to be least sensitive to the experimental uncertainty of the charged particle momenta. Fig. 3 shows the distribution of the square root of the sum of the p_T^2 for the events with at least 3 charged tracks in one hemisphere.

By analysing the events originating far from the interaction point (viz. $10 < |z| < 30$ cm) the contribution from beam gas events was found to be less than 0.1%. The two photon contribution was calculated by Monte Carlo simulation [6] and was also less than 0.1%. The $\tau^+\tau^-$ background was determined to be (1.3 ± 0.3)% using a Monte Carlo simulation performed with the event generator KORALZ [7].

For about 10% of the data some of the 12 sectors of the TPC were not read out by the data acquisition system. The selection criteria were chosen such that the results are rather insensitive to the incompleteness of these events. The events collected with the full TPC were used to determine a correction of (11 ± 1)% for this sample.

A detailed Monte Carlo simulation of the detector, which included secondary interactions, the collection of electronic signals and their digitization was performed. The event generation relied on the MUSTRAAL event generator [8] and on the Lund parton shower fragmentation model [9]. The simulation describes well the distributions of various topological variables of the hadronic data of DELPHI [10]. The same analysis was applied to the simulated and to the real events and good agreement between the two samples was observed.

For events with sphericity axes at small polar angles a lower efficiency was expected than for those in the barrel region (viz. $|\cos\theta| < 0.65$) where the efficiency was larger than 99.9%. The selection efficiency for

the full solid angle was obtained by extrapolating the theoretical shape $(1 + (1 - 8/3\ \alpha_s/\pi)\ \cos^2\theta_s)^{(*)}$ [11] of the sphericity axis distribution from the barrel region to small angles with $\alpha_s = 0.12$. Fig. 3(b) shows the sphericity axis distribution for data and Monte Carlo together with the fit to the data for $|\cos\theta_s| < 0.65$. Due to track losses in the forward region, the measured value of $|\cos\theta_s|$ was underestimated. The Monte Carlo simulation was used to correct the number of events in the barrel region for this effect by 3%. From this a total efficiency of $(93.5 \pm 1.0)\%$ was obtained. The various contributions to the uncertainty are summarized in Table 2.

TABLE 2 – Contributions to the uncertainty on the hadronic event selection efficiency

Error [%]	Analysis A	Analysis B
Theory and Monte Carlo	0.4	0.5
Data statistics	0.8	0.8
Uncertainty on momentum measurement	0.3	0.5
$\tau^+\tau^-$ contamination	0.3	0.1
Total	**1.0**	**1.1**

Analysis B:

For the second method, which consisted of a more severe selection than the previous one, charged particles were selected as above. In addition, clusters in the HPC which were not associated to charged particles were kept provided their energies were in the range $0.1 < E < 50$ GeV.

Hadronic events were accepted if the total charged multiplicity was at least 5 and if either the invariant mass of all charged particles was larger than 12 GeV, or the total energy (including the HPC clusters) was greater than 16 GeV. Figs 3(c) and (d) display the charged mass distribution for events having at least 5 charged tracks and the final charged multiplicity, compared with the same Monte Carlo simulation as above.

As in the previous analysis, the multiplicity cut removed cosmic and leptonic events, but the $\tau^+\tau^-$ contamination was reduced to $0.3 \pm 0.1\%$. The charged mass cut rejected the remaining contributions from beam gas and two photon interactions. The total energy cut improved the selection efficiency for full TPC data by 1%, and helped to recover most of the partial TPC runs. The efficiency correction for this data sample was $(13 \pm 1)\%$. The different sources of uncertainty are listed in Table 2.

The selection efficiency was derived from the simulation in the barrel region ($|\cos\theta_s| < 0.65$) and was then extended to the full acceptance. For this combined analysis, the total efficiency was $(92.1 \pm 1.1)\%$.

(*) The formula is calculated for the thrust axis. We checked with the Monte Carlo that it is also valid for the sphericity axis.

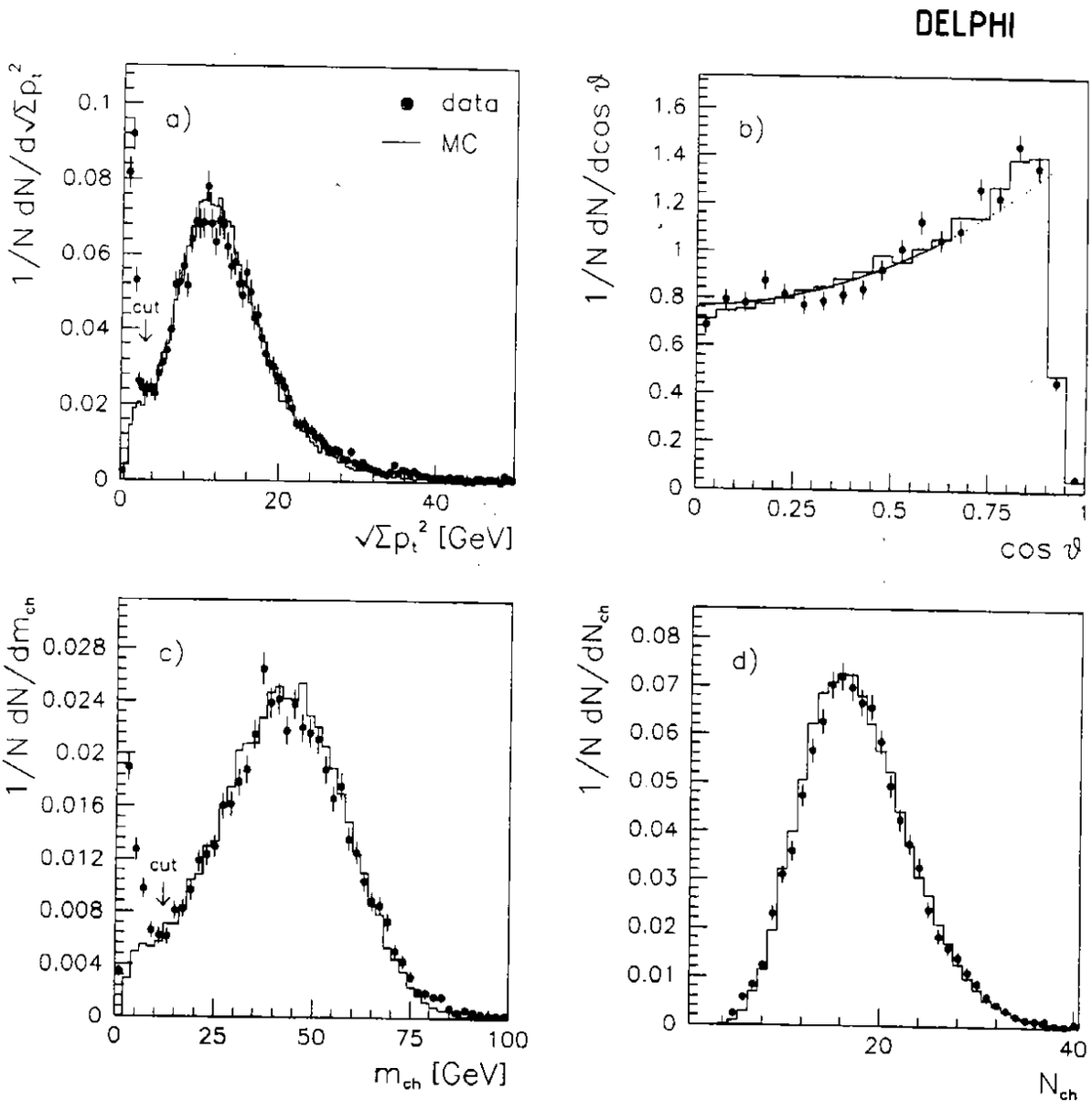

Fig. 3 – (a) Distribution of $\sqrt{\Sigma p_T^2}$ for events with ≥ 3 charged tracks in one hemisphere. Also shown is the Monte Carlo comparison (solid line) and the selection cut for analysis A.

(b) Sphericity axis distribution (data and Monte Carlo simulation) with a fit to the data (solid curve) and its extrapolation to small angles (dotted curve).

(c) Charged mass distribution for events with ≥ 5 charged tracks. Also shown is the Monte Carlo comparison (solid line) and the selection cut for analysis B.

(d) Final charged multiplicity distribution (analysis B) compared with the Monte Carlo simulation.

The uncorrected number of hadronic events selected by the two analyses are given in Table 3 for each center–of–mass energy. Once corrected for the global efficiency and for the $\tau^+\tau^-$ contamination the numbers of selected events for both analyses agree within 0.7% on average for each energy. The cross–sections computed in sect. 6 are based on the average results of both analyses.

TABLE 3 – DELPHI Z Scan with Hadrons

	# Hadronic events			
Collision energy [GeV]	Analysis A	Analysis B	Integ. L [nb^{-1}]	Cross–section(*) [nb]
88.284	241	236	54.4	4.74 ± 0.32
89.284	427	416	49.8	9.42 ± 0.50
90.283	1094	1060	61.8	19.51 ± 0.73
91.036	1987	1930	73.3	29.15 ± 0.89
91.283	2392	2321	81.9	31.02 ± 0.89
91.536	2984	2918	106.3	29.97 ± 0.76
92.286	785	768	39.8	20.92 ± 0.96
93.284	587	575	54.2	11.57 ± 0.55
94.284	280	270	35.0	8.54 ± 0.57
95.042	95	93	16.3	6.19 ± 0.69
Total	**10872**	**10587**	**572.8**	

(*) The errors do not include an additional systematic uncertainty of 2.6% on the overall normalization.

6. RESULTS

The hadronic cross–section was computed at each energy from the relation:

$$\sigma_h = \frac{N_Z - N_B}{L\varepsilon} \qquad (1)$$

where N_Z stands for the number of selected hadronic events, N_B is the number of background events, (viz. $\tau^+\tau^-$ events), L stands for the time integrated luminosity and ε is the overall efficiency for hadronic events.

The integrated luminosities and the cross–sections for each centre–of–mass energy are listed in Table 3. The quoted errors are statistical only. There is an additional energy independent normalisation uncertainty of 2.6%, of which 2.4% is due to the luminosity measurement and 1.0% is due to the determination of the total efficiency. The centre–of–mass energies are known with an absolute systematic uncertainty of 30 MeV and a point–to–point uncertainty of about 10 MeV [12]. The former is the main systematic uncertainty on M_Z in all the fits below whereas the effect of the latter is negligible.

The experimental line–shape was fitted with theoretical formulae in order to test the validity of the Standard Model and to determine the parameters of the Z resonance. We shall describe one of these formulae, viz. that of [13]. It consists of an "improved Born approximation" made of the sum of the two following terms:

– the pure continuum cross–section, $\sigma_\gamma(s)$, which includes its leading radiative correction.

– the cross–section for the resonance and interference terms, which can be expressed in a compact form as follows:

$$\sigma_Z(s) = 12\,\pi\,\frac{\Gamma_e\Gamma_h}{(s - M_Z^2)^2 + \frac{s^2}{M_Z^2}\Gamma_Z^2}\left[\left(\frac{s}{M_Z^2} + R\,\frac{s - M_Z^2}{M_Z^2}\right)F - (2 + R)G\right] \qquad (2)$$

where Γ_e and Γ_h stand for the electron and hadron partial widths of the Z. Γ_Z is its full width and M_Z its mass. Two–loop self–energy corrections to the vector–boson propagator are taken into account by the s^2/M_Z^2 and s/M_Z^2 terms. The function R includes mainly the contribution from the real part of the γZ interference computed to lowest order plus its leading logarithmic and leading top–quark mass corrections. Depending on the top quark and Higgs masses, it ranges from 0.07 to 0.12. A departure of the observed cross–section from the Standard Model prediction (due for instance to an additional Z boson) should manifest itself by an unexpected value of R. The functions F and G include mainly the radiative corrections: the soft part of the initial state photon radiation is taken into account by the exponentiation formalism of [14]; the hard part is computed to second order in α; final state radiation as well as its interference with the initial state radiation is taken into account at lowest order. The QCD corrections to the quark partial widths are computed to second order in α_s and amount to 4.0% (assuming $\alpha_s = 0.12$). A top quark mass of 130 GeV and a Higgs mass of 100 GeV were assumed.

Three fits were performed, starting with the least model dependent one and ending with the one most constrained by the Standard Model.

In the first fit Γ_Z, M_Z and the product of the partial widths $\Gamma_e\Gamma_h$ were left free to vary, in order to determine the total width without constraint from the overall normalisation of the data. The value of R was fixed to 0.095, corresponding to the top–quark and Higgs masses assumed above. The fits gave the following results:

$$\Gamma_Z = 2.511 \pm 0.065 \text{ GeV}; \qquad M_Z = 91.171 \pm 0.030 \text{ (stat.)} \pm 0.030 \text{ (beam) GeV};$$
$$\Gamma_e\Gamma_h = 0.148 \pm 0.006 \text{ (stat.)} \pm .004 \text{ (syst.) GeV}^2; \qquad \chi^2/\text{d.o.f.} = 4.0/6$$

The quality of the fit is good. The value of the Born cross–section at the pole $\sigma_0 = 12\pi\Gamma_e\Gamma_h/M_Z^2\Gamma_Z^2$ corresponding to the fitted values of Γ_Z, M_Z and $\Gamma_e\Gamma_h$ is:

$$\sigma_0 = 41.6 \pm 0.7 \text{ (stat.)} \pm 1.1 \text{ (syst.) nb}$$

The systematic errors on $\Gamma_e\Gamma_h$ and σ_0 follow from the 2.6% systematic error on the overall normalisation. The correlation between Γ_Z and σ_0 is illustrated in Fig. 4 where the fitted values of both parameters are shown with their 68% and 99% confidence level contours.

When the fit above was repeated with R free, the values of Γ_Z, M_Z and $\Gamma_e\Gamma_h$ remained essentially identical and R was found equal to -0.16 ± 1.02. Although this agrees with the expectations from the Standard Model, much higher statistics are needed for a conclusive test.

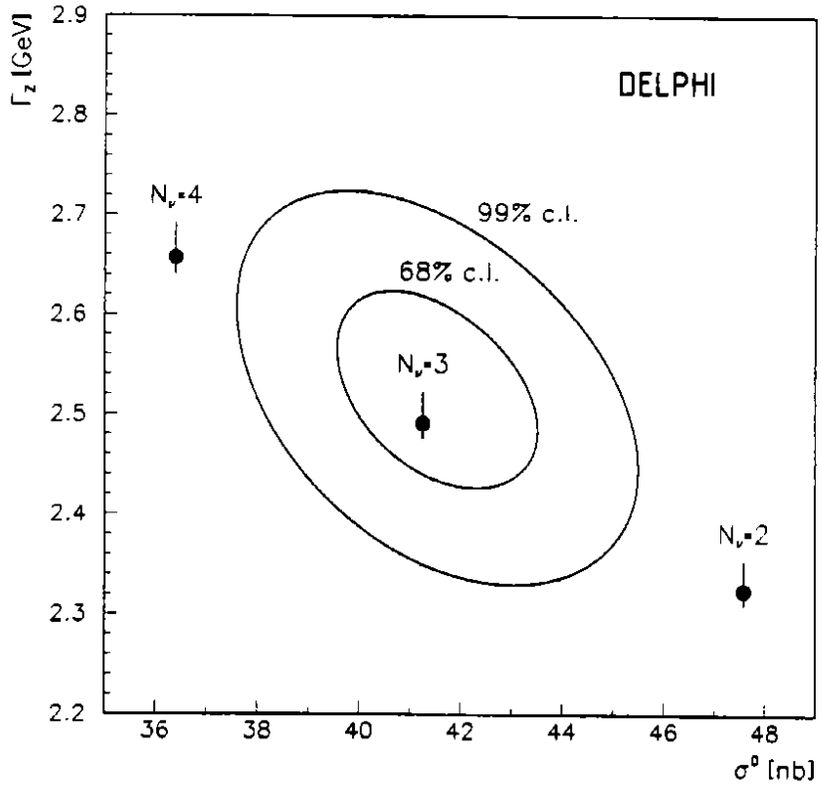

Fig. 4 – Contours of Γ_Z versus σ_0 for 68% and 99% confidence level. Also shown are the expected values for the number of massless neutrino species with their errors due to the uncertainty of the top quark mass (90–230 GeV) and the Higgs mass (10–1000 GeV).

In the second fit $\Gamma_e\Gamma_h$ is fixed to the value predicted by the Standard Model (viz. 0.146 GeV^2). The results are:

$$\Gamma_Z = 2.494 \pm 0.020 \text{ (stat.)} \pm 0.039 \text{ (syst.) GeV ;}$$

$$M_Z = 91.170 \pm 0.030 \text{ (stat.)} \pm 0.030 \text{ (beam) GeV;} \qquad \chi^2/\text{d.o.f.} = 4.0/7.$$

The systematic error quoted for Γ_Z originates from the 2.6% overall normalisation uncertainty. Using the partial widths from the Standard Model [15], we obtain an invisible width of $\Gamma_{inv} = 495 \pm 20$ (stat.) $\pm$ 39 (syst.) MeV and a corresponding number of light neutrino species of:

$$N_\nu = 2.97 \pm 0.12 \text{ (stat.)} \pm 0.23 \text{ (syst.)}$$

The error originating from the experimental uncertainty on the mass of the top quark and on the strong coupling constant amounts to less than 0.05 and has therefore been neglected. Combining the errors in quadrature, the fit excludes a fourth generation of massless neutrinos at a confidence level of 99.9%. A fourth neutrino with a mass smaller than 40 GeV is excluded at the 95% confidence level.

Finally a fit was performed where only M_Z and an overall normalisation factor K were left free to vary. All the other parameters were computed from the Standard Model assuming 3 massless neutrino generations. The results are:

$$M_Z = 91.171 \pm 0.030 \text{ (stat.)} \pm 0.030 \text{ (beam) GeV;} \quad K = 1.005 \pm 0.013; \; \chi^2/\text{d.o.f.} = 4.0/7$$

The quality of the fit shows that the Standard Model reproduces the data well. Fig. 5 displays the cross–section measured at each energy together with the result of the last fit (full line). The cross–sections predicted by the Standard Model for the same value of M_Z but for two and four massless neutrino species are also shown. One clearly observes that the data greatly favour three light neutrino species (as indicated by the fitted value of K). Due to radiative corrections, the peak maximum is about 100 MeV above the mass value. Thus the cross–section measured at 91.28 GeV can be considered as an experimental determination of the peak cross–section, viz. 31.02 ± 0.89 (stat.) $\pm$ 0.81 (syst.)nb, the systematic error originating in the overall normalization uncertainty.

Combining the results of the first fit with our measured ratio of the leptonic (flavour averaged) to hadronic widths $\Gamma_\ell/\Gamma_h = 0.0489 \pm 0.0023$ [16], we determined the leptonic and hadronic partial widths to be:

$$\Gamma_\ell = 85.1 \pm 2.9 \text{ MeV;} \qquad \Gamma_h = 1741 \pm 61 \text{ MeV;}$$

$$\Gamma_{inv} = 515 \pm 54 \text{ MeV.} \qquad \Gamma_h/\Gamma_\ell = 20.45 \pm .98$$

The errors include the systematic uncertainties taking into account all correlations. All values are in good agreement with the Standard Model. With the ratio Γ_ν/Γ_ℓ predicted by the Standard Model we derive the number of light neutrino species to be:

$$N_\nu = 3.05 \pm 0.28.$$

In this determination of N_ν, the theoretical uncertainty, which originates mainly from the unknown top quark mass, is negligible.

All the fits above were repeated with a different formulation of the cross–section [17]. The last fit was also performed with a more complete computation [18]. No difference was observed.

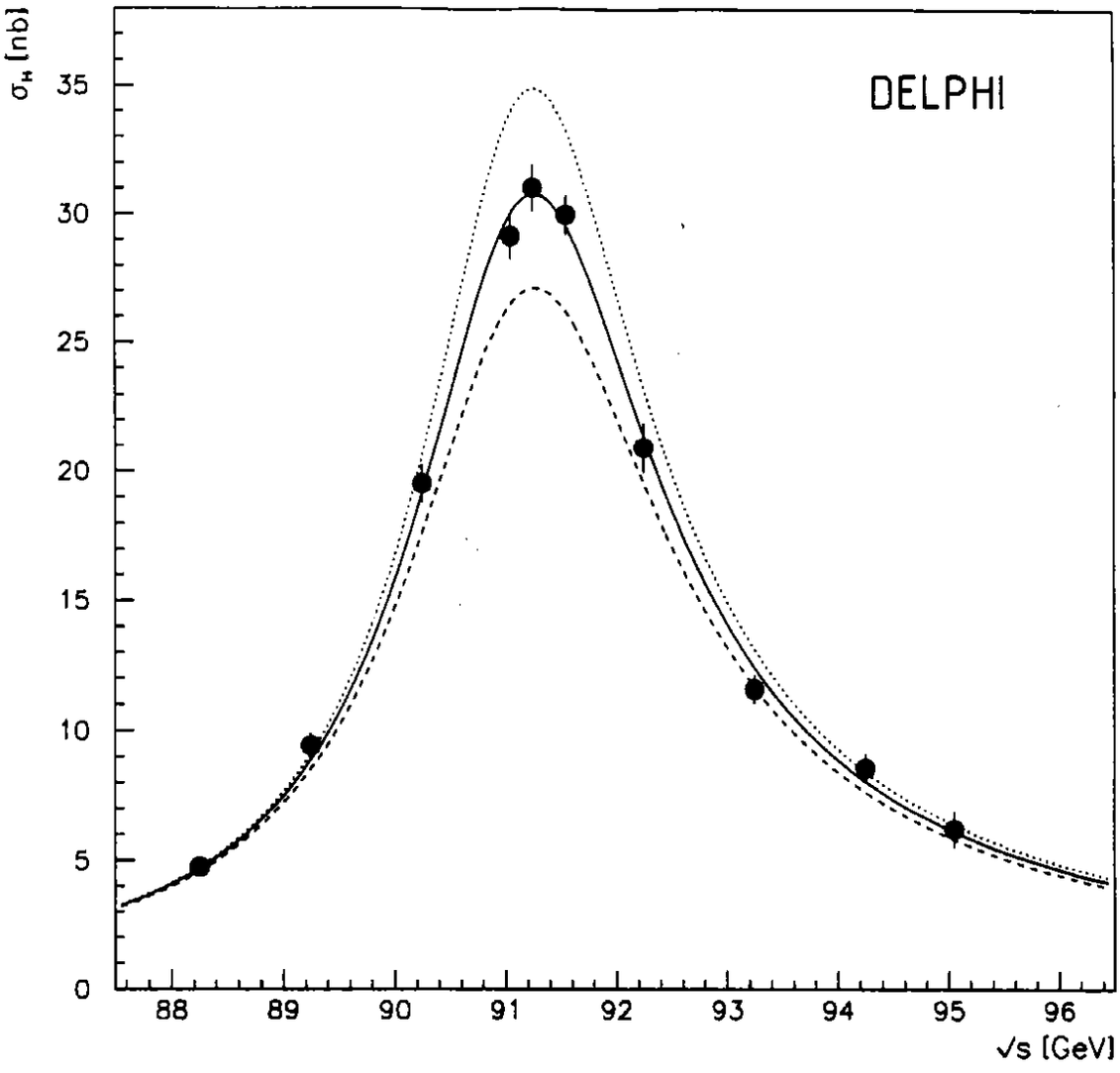

Fig. 5 – Cross section for $e^+e^- \to$ hadrons as measured at ten different energies together with the two parameter fit (M_z and overall normalization). Also shown is the cross section as predicted by the Standard Model assuming two (dotted line) and four (dashed line) massless neutrino species.

7. SUMMARY

On the basis of total samples of about 11000 hadronic decays of the Z boson and 17000 Bhabha events, corresponding to an integrated luminosity of 573 nb^{-1} recorded from October until December 1989 with the DELPHI detector, we have measured the line–shape of the Z boson at 10 different center–of–mass energies ranging from 88.28 to 95.04 GeV. The experimental line–shape has been compared to that predicted by the Standard Model. No disagreement was observed. Our results are also in agreement with other measurements [2].

The mass and the total width of the Z resonance are found to be

$$M_Z = 91.171 \pm 0.030 \text{ (stat.)} \pm 0.030 \text{ (beam) GeV}$$

$$\Gamma_Z = 2.511 \pm 0.065 \text{ GeV}.$$

The product of the electronic and hadronic partial widths and the corresponding unfolded cross–section at the pole are

$$\Gamma_e \Gamma_h = 0.148 \pm 0.006 \text{ (stat.)} \pm 0.004 \text{ (syst.) GeV}^2;$$

$$\sigma_0 = 41.6 \pm 0.7 \text{ (stat.)} \pm 1.1 \text{ (syst.) nb}.$$

The number of massless neutrino generations, assuming Standard Model couplings is

$$N_\nu = 2.97 \pm 0.12 \text{ (stat.)} \pm 0.23 \text{ (syst.)}.$$

The hypothesis of a fourth massive neutrino generation of less than 40 GeV is excluded with a confidence level of 95%.

From our measurement of $\Gamma_e \Gamma_h$ we derived the hadronic, leptonic and invisible widths:

$$\Gamma_h = 1741 \pm 61 \text{ MeV},$$

$$\Gamma_\ell = 85.1 \pm 2.9 \text{ MeV},$$

$$\Gamma_h/\Gamma_\ell = 20.45 \pm 0.98,$$

$$\Gamma_{inv} = 515 \pm 54 \text{ MeV}.$$

Acknowledgements

We are greatly indebted to our technical staffs and collaborators and funding agencies for their support in building the DELPHI detector and to the many members of LEP Division for the speedy commissioning and superb performance of the LEP machine.

REFERENCES

[1] DELPHI Collaboration, P. Aarnio et al., Phys. Lett. B231 (1989) 539.

[2] Mark II Collaboration, G.S. Abrams et al., Phys. Rev. Lett. 63 (1989) 724;
Mark II Collaboration, G.S. Abrams et al., Phys. Rev. Lett. 63 (1989) 2173;
L3 Collaboration, B. Adeva et al., Phys. Lett. B231 (1989) 509;
ALEPH Collaboration, D. Decamp et al., Phys. Lett. B231 (1989) 519;
OPAL Collaboration, M.Z. Akrawy et al., Phys. Lett. B231 (1989) 530;
ALEPH Collaboration, D. Decamp et al., Phys. Lett. B236 (1990) 399;
L3 Collaboration, B. Adeva et al., L3 preprint 4, December 1989, submitted to Phys. Lett. B.
OPAL Collaboration, M.Z. Akrawy et al., CERN/EP 90–27, February 1990, submitted to Phys. Lett. B.

[3] R. Brun, F. Bruyant, M. Maire, A.C. McPherson and P. Zanarini; 'GEANT3', CERN report DD/EE/84–1, September 1987.

[4] F.A. Berends and R. Kleiss; Nucl.Phys. B228 (1983) 537;
M. Böhm, A. Denner and W. Hollik, Nucl.Phys. B304 (1988) 687;
F.A. Berends, R.Kleiss and W.Hollik; Nucl.Phys. B304 (1988) 712.

[5] H. Burkhardt, F. Jegerlehner, G. Penso and C. Verzegnassi, Z. Phys. C43 (1989) 497.

[6] F.A. Berends, P.H. Daverfeld, R. Kleiss, Comp. Phys. Com. 40 (1985) 285–307.

[7] S. Jadach, B. Ward, Z. Was, R. Stuart, W. Hollick, to be published in Comp. Phys. Com. and Z Physics at LEP 1, vol. 3, CERN 898 (1989) 69–77.

[8] F.A. Berends, R. Kleiss, S. Jadach, Comp. Phys. Com. 29 (1983) 185–200.

[9] T. Sjôstrand, Comp. Phys. Comm. 27 (1982) 243; 28 (1983) 229.
T. Sjôstrand and M. Bengtsson, Comp. Phys. Comm. 43 (1987) 367.

[10] DELPHI Collaboration, P. Aarnio et al., CERN/EP 90–19, February 1990, submitted to Phys. Lett. B.

[11] J.H. Kühn et al., Heavy flavours at LEP MPI–PAE/PTh 49/89.

[12] A. Hoffmann, private communication.

[13] A. Borelli et al., CERN preprint TH 5441/89.

[14] M. Greco, G. Pancheri and Y. Srivastava, Nucl. Phys. B171 (1980); B197 (1982) 543.

[15] W.F.L. Hollik, DESY 88–188, to be published in Fortschritte der Physik.

[16] DELPHI Collaboration, P. Aarnio et al., CERN/EP 90–31, March 1990, submitted to Phys. Lett. B.

[17] ZAPPH, G. Burgers; 'Polarisation at LEP', Vol. 1, CERN 88–06, 121.
The computer program was provided by courtesy of G. Burgers.

[18] F.A. Berends et al., Nucl. Phys. B297 (1988) 429.
W. Beenakker and W. Hollik, CERN 87–08 (1987) 185.